# Enantiomer Differentiation by Interaction-Specific Prediction of Residual Dipolar Couplings in Spherical-like Molecules

David Elsing, Burkhard Luy, and Mariana Kozlowska*

**ABSTRACT:** Residual Dipolar Couplings (RDCs) are averaged dipolar couplings between nuclear spins of atoms in a molecule that can be measured by nuclear magnetic resonance (NMR) spectroscopy upon partial alignment by a chiral alignment medium. The estimation of differences in alignment of enantiomers may, in principle, enable the determination of absolute configuration. Here, we use molecular dynamics (MD) simulations to mimic the alignment of chiral molecules (i.e., isopinocampheol, quinuclidin-3-ol, borneol, and camphor) to the chiral poly-$\gamma$-benzyl-L-glutamate (PBLG) polymer to predict RDCs *in silico* and compare calculated and experimentally measured residual dipolar couplings for the four enantiomeric pairs. The aim is to validate the computational scheme for the prediction of RDCs in chiral molecules and understand the interaction leading to the alignment in more detail. We determine the indispensable importance of hydrogen bonds between a chiral molecule and the alignment medium on the overall quality of the simulated alignment and interaction poses toward high agreement with experiments. A good correlation with experimental data is found for camphor and isopinocampheol, while the correlation for quinuclidin-3-ol and borneol is lower. We attribute this observation to the high difficulty of the RDC prediction for rather almost spherical molecules. The study reveals that the prediction of alignment with small enantiomeric differences is possible with an MD-based approach; however, extended simulation times (e.g., 50−100 $\mu$s) are required to sufficiently reduce the statistical uncertainty. This may be further used for the determination of the relative, as well as absolute, configuration of chiral molecules.

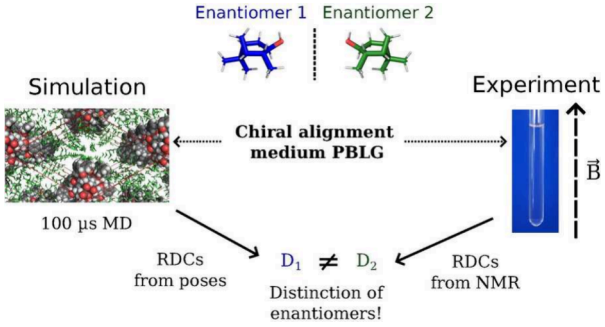


## INTRODUCTION

The chirality of organic molecules plays an important role in many chemical reactions and biological processes. The determination of absolute configuration of chiral organic compounds is a crucial task in chemistry and is still challenging. Although several methods for enantiomer differentiation or even measuring enantiomeric excess exist, such as X-ray diffraction for crystalline molecules,[1,2] electronic or vibrational circular dichroism (CD spectroscopy) for small molecules,[3,4] Coulomb explosion imaging or microwave three-wave mixing in the gas phase[5] and NMR spectroscopy on chirally derivatized compounds,[6] they all have severe limitations[7,8] and additional methods are in need. Chirally aligned NMR spectroscopy has a high potential to become such a method. In this type of NMR spectroscopy, a (chiral) analyte is partially aligned by a (chiral) alignment medium, which then allows the measurement of structurally valuable anisotropic NMR parameters.[9,10] The method already proved in a large number of studies with mostly nonchiral alignment media to be of high importance for the determination of relative configuration of organic molecules.[11−19] It is also well-established that residual dipolar couplings (RDCs) upon alignment to a chiral alignment medium may, in principle, allow for the determination of the absolute configuration of the analyte,[20−22] without the requirement of chemical modification of the analyte. As the average alignment in a chiral alignment medium depends on the chirality of the molecule of interest, different enantiomers result in different RDCs, making the method very powerful for the measurement of enantiomeric excess.[23]

For the special case that similar molecules with known chirality are available, even the absolute configuration could be determined[24] using cross-fitting.[25] A general approach based on theoretical calculation allowing the reliable prediction of RDCs in the chiral environment,is still missing however.[22]

RDCs are anisotropic NMR parameters, which depend on the distance between nuclear spins and the angle $\theta$ of the internuclear vector $\vec{r}_{ij}$ to the static magnetic field (see Figure 1a). They are proportional to $\langle(3\cos^2(\theta)-1)/r_{ij}^3\rangle$, where the averaging expands over a full experimental free induction decay

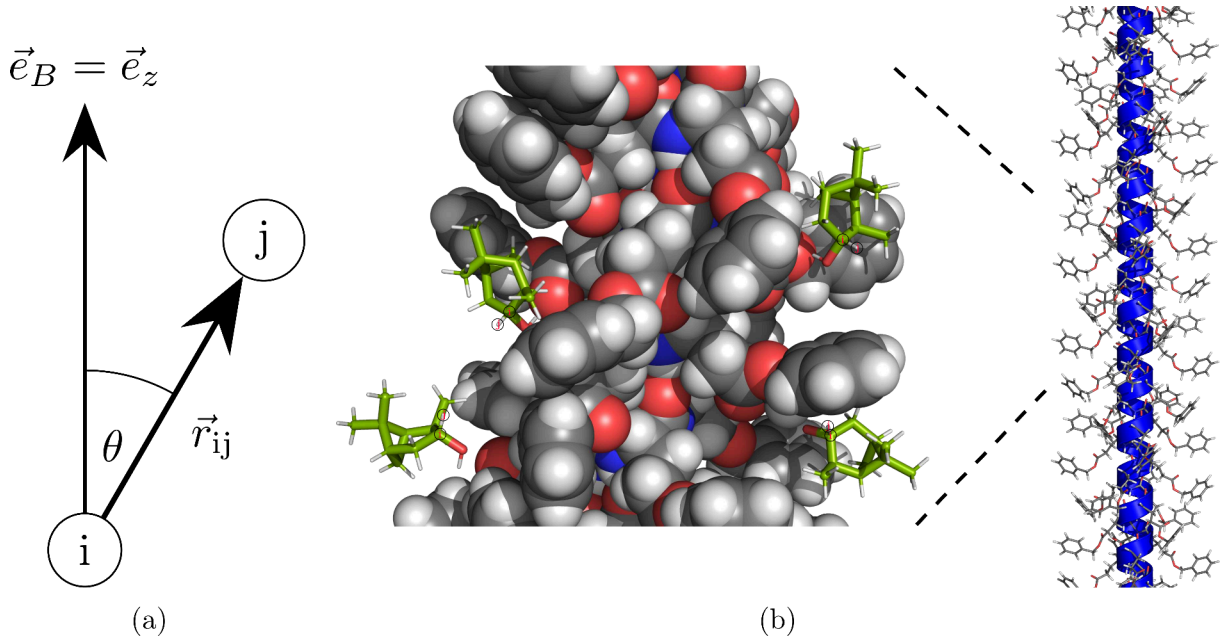


**Figure 1.** Schematic representation of RDC calculation and its application to PBLG polymer. In (a), a representation of the relative positions of two nuclei $i$ and $j$ in a molecule is depicted. The RDC is determined by the average over their distance $\vec{r}_{ij}$ and the angle $\theta$ to the external magnetic field. In (b), different poses of (−)-isopinocampheol near PBLG are illustrated. Through the interaction with the alignment medium, the overall movement of the analyte and thus of the atom pairs within the molecule for which the RDCs are measured (here $i$ and $j$ as in (a)) becomes anisotropic. Solvent molecules are not shown. Note that in the actual MD simulations, only one analyte molecule per box is present.

(FID), which is typically larger than 100 ms. The target is then to predict the averaged alignment with a molecular model to such accuracy that differences in alignment for a pair of enantiomers are determined.

While RDCs are straightforwardly used for structure prediction of proteins[26,27] and other macromolecules,[28] the prediction of alignment for small molecules is far more difficult, as the fine details of alignment medium to solute interactions need to be treated accurately.

Simple methods for the prediction of RDCs by an alignment medium include the averaging of the alignment by steric exclusion and electroctrostatic interation with a (charged) wall or cylinder (PALES)[29,30] or approximations thereof.[31−33] More recently, Opakua et al.[16] demonstrated a relatively simple model (called P3D) for the estimation of RDCs for diastereomers of rigid molecules (e.g., 4,6-diacetylhygrophorone A, strychnine or isopinocampheol).[16,34] There, the correct assignment of diastereometers was accomplished by using a precomputed electrostatic potential of the aligning polymer based on the Poisson equation and steric exclusion by modeling atoms as hard spheres. However, theoretical methods reported have not shown conclusive differences in RDCs of enantiomers usable for the assignment of absolute configuration.[22,35]

Other methods for alignment prediction are based on molecular dynamics simulations. For the alignment of analyte organic molecules in a nematic solvent, Pizzirusso et al.[36] used all-atom MD simulations to predict the order parameter $\langle P_2 \rangle$, which was demonstrated to correlate with measured dipolar couplings in NMR. Frank et al.[37] have shown stochastic MD simulations using Langevin dynamics of strychnine aligned by a polystyrene/$CDCl_3$ gel to predict RDCs. In the relatively simple model, a single polymer strand fixed along the axis of alignment (the $z$-axis) was used and a quite good correlation between simulated and experimental values could be shown. However, none of the approaches could show the differentiation of enantiomers so far.

Here, we will show results of an attempt to predict the alignment to an accuracy that allows the distinction of enantiomers. It is based on the model of Frank et al.,[37] but expanded by careful choice of parameters and including explicit solvent molecules. Among the different known chiral alignment media,[38−41] the most important one is the liquid crystalline phase poly-$\gamma$-benzyl-L-glutamate (PBLG), which formed the basis for most developments regarding the distinction of enantiomers.[42,43] We therefore chose a PBLG/$CDCl_3$-based model for our study and focused on solutes of a recently accepted study of small rigid molecules performed in one of the author's laboratory with detailed access to experimental data[44] and on the similar, well-studied molecule isopinocampheol.[42,45] We will present the results of the various models and analyze the important factors of intermolecular interactions that are responsible for alignment.

## THEORY

**Residual Dipolar Coupling.** For a pair of nuclear spins $I_1$ and $I_2$ in a molecule, the secular, weak coupling Hamiltonian in a strong static magnetic field $B$ aligned along the $z$-axis is given by

$$\hat{H} = \hbar[\omega_1 \hat{I}_{1,z}\hat{\mathbf{1}}_2 + \omega_2 \hat{\mathbf{1}}_1 \hat{I}_{2,z} + 2\pi(J_{ij} + 2D_{ij})\hat{I}_{1,z}\hat{I}_{2,z}] \quad (1)$$

Here, $\omega_i = \gamma_i B(1 + \delta_i)$ is the Larmor frequency of spin $i$ with gyromagnetic ratio $\gamma_i$ and chemical shift $\delta_i$. The secular approximation assumes that the interaction with the large static magnetic field dominates. Moreover, it is assumed that the averaging of the molecular orientation occurs on a smaller time scale (picoseconds to milliseconds[46]) than the relaxation time scale. The last term in eq 1 introduces a coupling between the two spins, which leads to a transfer of transverse magnetization

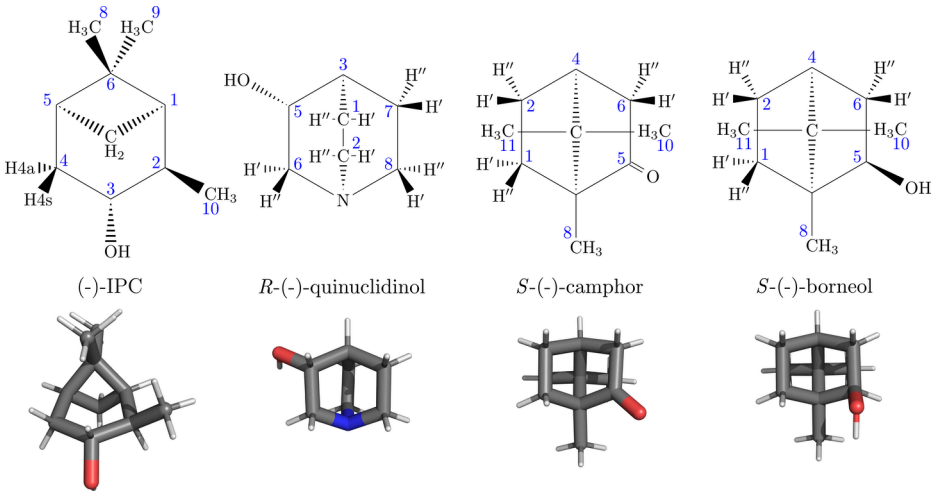


**Figure 2.** Visualization of one enantiomer for each of the four chiral molecules isopinocampheol ("(−)-IPC"), quinuclidin-3-ol ("*R*-(−)-quinuclidinol"), camphor ("*S*-(−)-camphor") and borneol ("*S*-(−)-borneol"). The respective other enantiomer is the point reflection of the structure shown here. We use the same numbering as in Marxet al.[42] and Sager et al.[44]

and thus a measurable peak splitting of $|J_{ij} + 2D_{ij}|$.[47] It consists of the dipolar splitting contribution, $2D_{ij}$, i.e. through the direct dipole−dipole interaction of the spins (the dipolar coupling constant is half the splitting contribution) and the scalar (or *J*-) coupling, $J_{ij}$, mediated through chemical bonds.

If the molecular orientation is isotropically distributed, the averaged dipolar couplings vanish. However, under anisotropic conditions, e.g. by the interaction with an alignment medium, they remain nonzero (albeit much reduced in magnitude compared to a fully aligned solid). Given sufficiently weak alignment, the $J_{ij}$-coupling has negligible anisotropy and thus remains unchanged.[48] Therefore, the residual dipolar coupling can be obtained directly by comparing the splitting between the isotropic and anisotropic case. If $|2D_{ij}| < J_{ij}$, as is the case for the experimental data referenced here, it can be uniquely obtained from the measured $|J_{ij} + 2D_{ij}|$.

In addition to the experimental measurement of $2D_{ij}$ using NMR spectroscopy, the coupling $D_{ij}$ can be calculated from the internuclear vector $\vec{r}_{ij}$ between the nuclei *i* and *j* of the molecule studied using the following equation:[49]

$$D_{ij} = -\left\langle \frac{3\gamma_i\gamma_j\mu_0\hbar}{16\pi^2 r_{ij}^3} \underbrace{\left(\cos^2(\theta) - \frac{1}{3}\right)}_{=P_2(\cos(\theta))} \right\rangle_t \tag{2}$$

where $\theta$ is the angle between $\vec{r}_{ij}$ and the static magnetic field (see Figure 1a), $\mu_0$ is the vacuum magnetic permeability and $P_2(x)$ is the second Legendre polynomial. If the correlation between $r_{ij}$ and $\theta$ is assumed to be negligible, e.g. for bonded nuclei where the time scale of bond vibrations is small,[50] $r_{ij}$ can be replaced by its average value. In the present work, this approximation is separately validated by taking $r_{ij}$ from each trajectory frame in MD simulations or from a fixed reference structure. It is described in the Results section.

**Alignment Tensor.** In a rigid molecule, all angle parameters can be expressed by a single symmetric and traceless tensor of order 2. It is commonly called alignment tensor *A* or Saupe matrix (if scaled by a factor $\frac{3}{2}$). For an internuclear unit vector $\vec{r}$, it is defined as

$$\langle \cos^2(\theta) \rangle_t - \frac{1}{3} = \vec{r}^{\,\mathrm{T}} A \vec{r} \tag{3}$$

where $\theta$ is the angle of $\vec{r}$ to the external magnetic field (here along the *z*-axis).[49] Given the rotation matrix $R_t$ from the reference structure to the pose of the chiral molecule with respect to the alignment medium at time *t*, the alignment tensor is given as

$$A = \frac{1}{3}\left\langle R_t^{\mathrm{T}} \begin{pmatrix} -1 & 0 & 0 \\ 0 & -1 & 0 \\ 0 & 0 & 2 \end{pmatrix} R_t \right\rangle_t \tag{4}$$

When considering a fixed reference structure of a rigid analyte molecule, the five independent components of *A* can be fit by linear least-squares to a set of RDCs.[11,51] As the molecules in this work are quite rigid, we have used a single optimized structure optimized as a reference shown in Figure 2. They were optimized by density functional theory (DFT) with the B3LYP functional[52] and the def2-SVP basis set,[53] using `PySCF`.[54] To make a comparison between enantiomers possible, we only optimized one enantiomer and used its point reflection as the reference structure for the other enantiomer.

**Comparison to Experiment.** The experimental RDCs are determined by measuring the distance between doublet components in CLIP/CLAP-HSQC (clean in-phase/clean antiphase heteronuclear single quantum correlation)[55] and P.E.HSQC (primitive and exclusive HSQC)[56] experiments, which are split by the *J*-coupling and the RDCs.[45] Their uncertainty is estimated from experimental data by left and right peak slope differences relative to the signal-to-noise ratio of spectra as described in Kummerlöwe et al.[25] The concentration and exact degree of alignment along the magnetic field of PBLG is unknown,[42,45] but is strongly correlated with the quadrupolar coupling.[57] Thus, the theoretical predictions, where the PBLG molecule is perfectly aligned along the *z*-axis (as depicted in Figure 1b), can be compared to the experimental values up to a constant factor as long as the anisotropy is in the *z*-direction (as explained in the Supporting Information, SI). This assumption was also applied

for stretched gels as alignment medium,[37] using a similar simulation setup to the polymer studied here.

As the scaling factor between the two sets of RDCs, $\vec{D}_1$ and $\vec{D}_2$, originated from *in silico* simulations and experiments, respectively, would be rather hard to predict, because it depends on the concentration and distribution of the PBLG chains, their average orientation along the *z*-axis and the fraction of time the analyte molecules interact with the PBLG side chain, they can be compared by the cosine similarity:

$$S = \frac{\vec{D}_1 \cdot \vec{D}_2}{\|\vec{D}_1\| \|\vec{D}_2\|} \tag{5}$$

The Pearson correlation coefficient, which is commonly used to compare predicted and measured RDCs,[58] is not entirely adequate for this purpose, because it is unchanged for a constant offset between the two sets of RDCs, while they should be related only by a constant factor without an offset. Therefore, in the present study, we use the cosine similarity, as only the values close to $S = +1$ indicate good agreement between two sets of RDCs. We visualize $|S|$ instead of $S$ in the following to make the values near $S = +1$ better visible.

## COMPUTATIONAL DETAILS

Encouraged by previous MD simulations to calculate RDCs in chiral analyte molecules aligned by an alignment medium,[37,45] we simulated the alignment of the four pairs of chiral molecules, i.e. isopinocampheol, quinuclidin-3-ol, borneol and camphor (depicted in Figure 2) by PBLG in chloroform. All four molecules represent small, bridged and therefore quite rigid entities, that are readily available as enantiomerically pure compounds. IPC is a well-known model compound for RDC measurements[42,59,60] and the other three compounds were chosen in a study to look at the influence of H-bond donor and acceptor groups.[44,45] Additionally, quinuclidinol contains a nitrogen H-bond acceptor as well.

It was shown experimentally that analyte molecules interact with multiple chains of PBLG[59,61] during the measurement time, although this does not per se rule out large residence times at the binding sites. We thus expect a significant number of distinct interaction events in the course of a dwell time, which is typically on the order of 100 $\mu$s. In addition, in Frank et al.,[37] it was suspected that the explicit treatment of solvent molecules might be important for the accurate description of the alignment. These previous calculations, using only Langevin dynamics and no solvent molecules, showed that the analyte molecules attach very strongly to the alignment medium in the local energy minima. Even though the difference of the alignment induced by PBLG of IPC in several halogenated solvents was found to be relatively small,[37,59] it is known from NMR experiments that molecules show fast exchange averaging on the acquisition time scale.[59] For a more realistic description of the solvent effects, we chose explicit solvation by chloroform for the simulations. The poses of the chiral solute molecules in the presence of PBLG, sampled in MD, were then used to calculate RDCs.

**Simulated Molecular Systems.** In nonpolar organic solvents, the backbone of PBLG is considered to be highly stabilized by the multitude of intrahelical H-bonds formed. As such, specific H-bond interactions with the analyte are only possible at the side chains and the simulation of a single PBLG chain is expected to be a good approximation. For the PBLG model, we used the approach described in Helfrich et al.[62] and Helfrich and Hentschke,[63] where it is represented as a 18/5 $\alpha$-helix with 18 residues connected across periodic boundary conditions. To build the PBLG polymer model, we first started with a single benzyl-L-glutamate (BLG) monomer, capped by $COCH_3$ and $NHCH_3$ groups (see Figure S1(a)). The molecules were then optimized with the B3LYP functional[52] and def2-SVP basis[53] set using `PySCF`[54] with the `XCFun`[64] and the `geomeTRIC`[65] libraries. Afterward, the bond lengths, angles and dihedrals of the backbone were adjusted to fit the experimentally determined structure of an 18/5 $\alpha$-helix of $\alpha$-poly-L-alanine,[66] see Figure S1(b). The PBLG molecule was modeled as a sequence of 18 BLG repeat units of 2.7 nm length,[62,67] periodically connected across the periodic boundary conditions to mimick an infinite long chain. After equilibration, this resulted in the simulation box depicted in Figure 3.

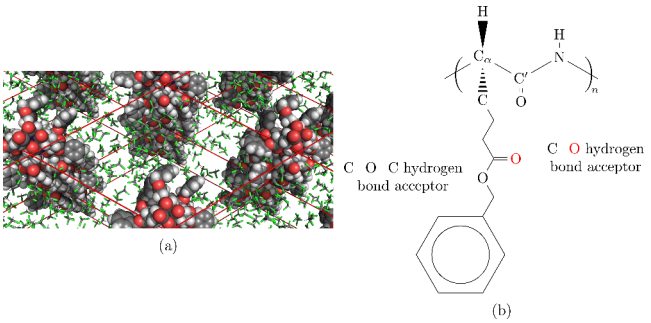


**Figure 3.** (a) Simulation box of PBLG and chloroform along the *z*-axis (without analyte molecule). For better visibility, only two periodic images in the *z*-direction and every third chloroform molecule are shown. The PBLG atoms are represented by their van der Waals surface. (b) Chemical structure of PBLG indicating the two potential hydrogen bond acceptors in the amino acid side chain. Only the C═O acceptor is capable to form strong H-bonds with an analyte.

**Force Field Parameters.** The 3D structure of the capped BLG monomer was generated using RDKit[68] and subsequently optimized by DFT in the same manner as the analyte molecules. The partial charges for all molecules were obtained by a restrained electrostatic potential (RESP) fit[69] to the electrostatic potential in vacuum obtained by the Hartree–Fock calculation with `PySCF`[54] using the 6-31G*basis set[70−72] (consistent with the AMBER methodology). In the RESP fit, the total charges of the BLG monomer and both caps were restrained to zero, respectively.

All noncharged force field parameters were obtained using `AmberTools 21`.[73] The assignment of atom types in the force field was done automatically using the `antechamber`, `parmchk2` and `tleap` programs from `AmberTools`. For PBLG, the AMBER ff14SBonlysc force field was used, while the GAFF (Generalized AMBER Force Field)[73] force field was used for the analyte molecules. For chloroform, we used the parameters from Fox and Kollman.[74] Since a single (capped) monomer does not contain all force field parameters needed for the polymer, the automatic assignment of the force field parameters for PBLG with `AmberTools` was done for an oligopeptide with three monomers and the same caps (shown in Figure S1(c)). The values used for the polymer were then taken from the parameters involving the atoms in the central monomer.

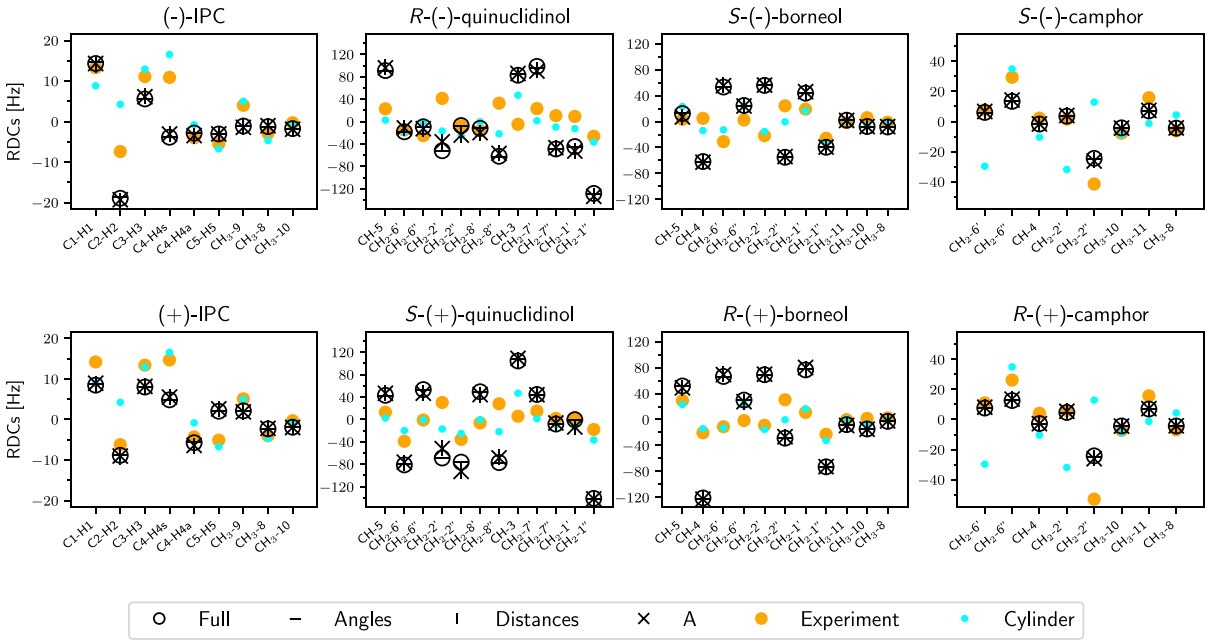


**Figure 4.** Residual dipolar couplings ($2D_{ij}$) of the chiral analytes calculated for four pairs of enantiomers. The different ways the RDCs were calculated ("Full", "Angles", "Distances" and "A") are described in the text. The RDC values obtained by replacing PBLG by a cylinder (i.e., without force field, as implemented in the PALES model[30]) are shown in cyan. RDCs calculated based from MD data and the cylinder approximation of the PBLG were scaled to the experimental RDCs (in orange) by the ratio of the sum of the squared RDCs, where the scaling for each enantiomer pair was averaged. Thus, the scaling is the same for both enantiomers.

**Molecular Dynamics Simulations.** All MD simulations were performed using GROMACS 2022.2.[75] To convert and construct the topologies with the force field parameters, the ParmEd library[76] was used. For all simulations, the time step using the Velocity-Verlet integrator[77] was set to 2 fs. For the short-range electrostatic and van der Waals contributions, a cutoff of 1.2 nm was chosen, while the long-range electrostatic contributions were calculated with the particle mesh Ewald method.[78] To set the simulation temperature, the velocity rescaling thermostat, as reported by Bussi et al.,[79] was used with a reference temperature of 300 K. Also, the length of molecular bonds involving hydrogen atoms were constraint using the LINCS algorithm[80] with order 4.

An initial periodic cubic box of chloroform with dimensions of 5.12 × 5.12 × 5.12 $nm^3$ was created with a density of 1.48 $g/cm^3$.[81] It was subsequently minimized to a maximum force of 100 $kJmol^{-1}nm^{-1}$ and equilibrated in the NVT ensemble with fixed box vectors over 100 ps. Afterward, NPT equilibration with the stochastic cell rescaling barostat[82] over 200 ps and finally NPT equilibration with the Parrinello–Rahman barostat[83] over 1 ns was performed. For both NPT simulations, a compressibility of 1.086 $\cdot 10^{-4}$ $bar^{-1}$ and a reference pressure of 1 bar were chosen and long-range dispersion corrections for energy and pressure were applied.[84] For the stochastic cell rescaling barostat, the relaxation time constant was set to 1 ps to avoid instabilities due to the initial state, while a time constant of 5 ps was chosen for the Parrinello–Rahman barostat. The final density (which is determined by the force field parameters) was 1.49 $g/cm^3$, slightly higher than the experimental value of 1.48 $g/cm^3$[81] at 25 °C.

The remaining molecular systems were solvated using this solvent box. This resulted in 172–174 chloroform molecules finally included in the simulation box. Here, the thermostat was applied separately to the solvent and the solutes (PBLG or PBLG + analyte molecule). The energy minimization and NVT equilibration were performed similarly as for the chloroform box explained above, but the NPT equilibration was done only with the Parrinello–Rahman barostat for 1 ns for the periodic PBLG chain. For the systems with periodic PBLG, the pressure coupling was only applied in the *xy*-directions.

For the MD simulations involving PBLG, the box size was chosen to preserve the feasible statistical convergence of observables, avoiding significant interaction between periodic images. It was defined by a hexagonal lattice in the *xy*-plane with a spacing of ∼3.5 nm, whereas the *z* lattice vector was orthogonal to the *xy*-plane and of length 2.7 nm. The size of the simulated box was also selected in the way allowing the chiral solute molecule to move freely within the box, avoiding interactions with the periodic image. PBLG as a liquid crystalline phase ordered along the magnetic field[85] may have stabilizing interhelical interactions. They should however occur only sporadically, following the assumption that interactions of the solute with a single PBLG chain are dominant.[86] Therefore, we have modeled the PBLG-based alignment medium by a PBLG $\alpha$-helix pointing along the *z*-axis in a box of explicit chloroform. We confirmed this choice by performing additional simulations with two PBLG $\alpha$-helices in the simulation box (as explained in the SI).

MD simulation runs with a total simulation time of 100 $\mu$s for each analyte in the presence of PBLG were performed as 1000 parallel MD simulations with a respective length of 100 ns each. In each of the simulations, a single analyte molecule was inserted randomly inside the PBLG/chloroform box using the gmx insert-molecules command in GROMACS, replacing overlapping solvent modules and avoiding clashes with PBLG by retrying. The initial velocities of all atoms in each simulation were prepared with a different pseudorandom number generator seed. In all cases, the initial MD production

run was preceded by an energy minimization and NVT equilibration over 200 ps as for the other systems. The production MD simulations were then performed with identical parameters as for the NPT equilibration of the system with periodic PBLG alone, where the trajectory for the analysis was saved every 10 ps. To reduce the bias due to the nonensemble distribution from which the initial states are prepared, each of the 1000 parallel MD chains was equilibrated for 1.1 ns before the actual MD runs. This suffices, as there are no large conformational changes of PBLG and the system without an analyte molecule is invariant under a shift along and a rotation around the $z$-axis by one monomer.

**Automated Workflow.** For automating the MD simulations and analysis of the data obtained from 1000 parallel runs, the `Snakemake` workflow management system[87] was used for all steps, including the preparation and the analysis described below. The employed software was built with the `GNU Guix` package manager.[88] The workflow protocol ensures consistent and self-contained calculation steps for all molecules and the reproducibility of all simulations. It is available under https://gitlab.kit.edu/david.elsing/RDCMD.

For reading the MD trajectories and fitting a rotation matrix from the analyte molecular reference structure to their orientation during the simulation, the `MDAnalysis` library[89,90] was used.

**Calculation of RDCs from MD.** RDCs were calculated from the saved MD trajectories according to eq 2. To investigate the importance of molecular flexibility, the $r_{ij}$ and angles were both taken from the trajectory directly or alternatively from the rotated reference structure. This is described in more detail below. Due to the fast rotation of the $CH_3$ groups,[91] the RDCs were calculated based on the orientation of the carbon atom and the neighboring non-hydrogen atom instead (refer to the SI for more details). In Marx et al.,[42] the C8−C6, C9−C6 and C10−C2 couplings in IPC (labels of atoms are depicted in Figure 2) were originally measured as $CH_3$ groups and then converted to C−C couplings based on the prefactor in eq 2. To compare them with the other RDC data only containing C−H couplings, we converted them back to the C−H RDC values and used the error estimate (scaled by the same factor) from Figure 4 in Marx et al.,[42] assuming a C−H bond length of 1.1 Å and a C−C bond length of 1.54 Å. For quinuclidinol, borneol and camphor, we use the assignment of the RDCs to the molecular structure found in Sager et al.[44] There is however a discrepancy for the C8−C6 and C9−C6 couplings in (+)-IPC between Marx et al.[42] and Sinnaeve et al.[60] (in this report, they are called C8−H8 and C9−H9), where the assignment is swapped. As there is little information on the assignment in Marx et al.,[42] the RDCs of the enantiomers should be close and an alignment tensor fit to our reference structure clearly favors the latter assignment, we swap the assignment also for (−)-IPC.

**Statistical Analysis.** Since the partial alignment of chiral molecules by PBLG is expected to be rather weak and the average values of the RDCs are much smaller in magnitude than their instantaneous values, a robust estimation of the statistical uncertainty was necessary. We have used the adjusted initial sequence estimator ("mISadj") from Dai and Jones[92] to estimate the asymptotic covariance matrix of the average, assuming the validity of the Markov chain central limit theorem.[93] It guarantees a positive definite covariance matrix and a (slight) overestimation of the eigenvalues of the covariance matrix, given that the state space is sufficiently sampled. The estimator $\hat{\Sigma}$ is based on the expression of the covariance matrix in terms of the autocorrelation function $\gamma_t$ according to

$$\hat{\Sigma} = -\gamma_0 + 2\sum_{t=0}^{\infty}(\gamma_t + \gamma_{-t}) \tag{6}$$

where $\gamma_t = \gamma_{-t}{}^{\mathrm{T}}$ is estimated by

$$\hat{\gamma}_t = \frac{1}{n}\sum_{i=1}^{n-t}(X_i - \hat{\mu}_n)(X_{i+1} - \hat{\mu}_n)^{\mathrm{T}} \tag{7}$$

for $t \in \{0, \ldots, n-1\}$ . In eq 7, the $X_i$ are the samples in the Markov chain, $n$ is the number of samples and $\hat{\mu}_n = \sum_{i=1}^{n} X_i/n$. Although this estimator is only defined for a single Markov chain, it can be trivially extended to multiple, independent chains (like the 1000 independent MD trajectories in our case) as long as the beginning and end of each chain are statistically independent. This assumption is valid in the case studied here, because the length of each chain (100 ns) is much longer than the lifetime of the "bound" configurations (i.e., interaction pose with chiral molecule and PBLG, see SI). Moreover, the system without the analyte molecule (i.e., PBLG by itself) is, on average, symmetric upon moving along the polymer repeat unit and rotating around the $z$-axis. Therefore, the estimator for the autocorrelation function, used in eq 6, for $N$ such chains is

$$\hat{\gamma}_t = \frac{1}{\sum_{k=1}^{N} n_k}\sum_{k=1}^{N}\sum_{i=1}^{n_k-t}(X_{k,i} - \hat{\mu}_{k,n_k})(X_{k,i+1} - \hat{\mu}_{k,n_k})^{\mathrm{T}} \tag{8}$$

where $n_k$, $X_{k,i}$ and $\hat{\mu}_{k,n_k}$ are defined for chain $k$ as in eq 7. This analysis was used to determine the statistical uncertainty of the calculated averages. Thus, it could be ensured that the calculated RDCs are sufficiently converged.

## RESULTS AND DISCUSSION

For this pioneering work, we have used four experimentally studied chiral molecules, i.e. isopinocampheol, quinuclidin-3-ol, borneol and camphor. Their two-dimensional and three-dimensional structures are visualized in Figure 2. The molecules were selected mostly due to the available experimental RDC data for both enantiomers and that they are rather rigid, which allows fitting of the alignment tensor without the need for an accurate description of the flexibility of molecules by the force field. Since the chiral molecules selected are all spherical-like, the alignment is weak, which makes the measurement of RDCs more feasible,[94] but the *in silico* prediction more challenging and computationally expensive. Moreover, we aimed to estimate the role of the specific interaction between the analyte and the alignment medium, therefore, isopinocampheol, quinuclidin-3-ol and borneol were selected due to the presence of a single O−H hydrogen bond donor. It is expected to interact with the hydrogen bond acceptor(s) in PBLG[86] (see Figure 3), which may impact the RDCs and induce differences between enantiomers. Additionally, camphor was selected as another previously studied pair of enantiomers with a very similar structure to borneol, except with a carbonyl group instead of the hydroxyl group, i.e. the H-bond donor is missing in this case. This allows for the investigation of the influence of hydrogen bonds on the partial alignment and the enantiomer specificity on the RDCs.

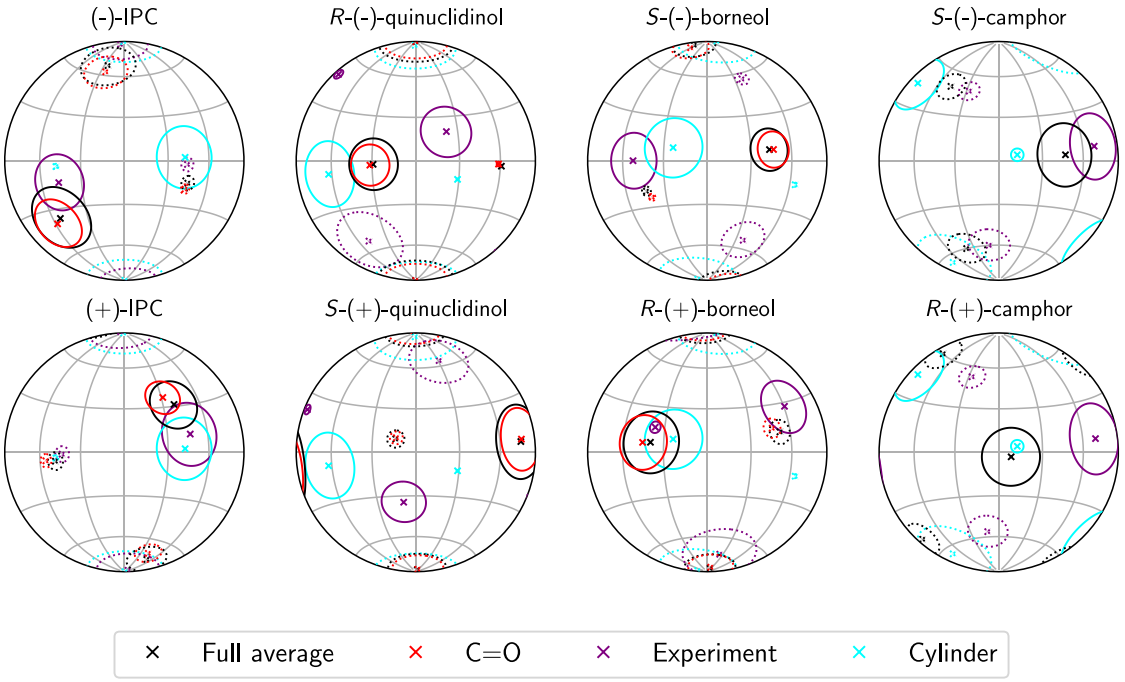


**Figure 5.** Eigenvectors and eigenvalues of the alignment tensor (defined in eq 4 and fitted for the experimental one) for the eight molecules aligned by the PBLG polymer. The eigenvectors are indicated by the × markers on a hemisphere, while the corresponding eigenvalues are represented by circles around the position of the eigenvectors. The area of the circles is proportional to the absolute value of the eigenvalue. Dashed lines indicate a negative sign and solid a positive sign of the eigenvalue. The black and red colors indicate values from MD ("Full" and of poses with C=O donor) normalized by the total simulation time, whereas the cylinder prediction is shown in cyan and experimental values are in purple.

**RDCs of Chiral Molecules.** The RDC values for the chiral molecules, shown in Figure 4, were calculated from MD simulations using eq 2 in several ways: (i) taking both distances and angles from the trajectory (labeled as "Full"), (ii) taking only the angles from the trajectory and the distances from the DFT-optimized reference structure (labeled as "Angles"), (iii) taking the distances from the trajectory and the angles from the rotated reference structure (labeled as "Distances"). In the last two cases, the rotation of the reference structure was fitted to the positions in the trajectory by minimizing the RMSD of the positions using the `MDAnalysis` library, and the distances or angles were taken from the rotated reference structure instead of the trajectory directly. In addition, the RDCs obtained by using only the alignment tensor (eq 4) averaged over the rotation of the reference structure (labeled as "A") are shown in Figure 4 as well. To compare RDCs originated from MD to the established PALES approach,[30] which is an approximation to predict the alignment tensor representing the alignment medium as a cylinder, we have calculated the RDC values from the alignment by steric exclusion with a cylinder of radius 10 Å. Here, we calculated the respective RDCs from the alignment of the rigid reference structure using naive Monte Carlo integration over rotations and translations. They are marked in cyan in Figure 4 and labeled as "Cylinder". The RDCs from experiment and the scaled RDCs from MD simulations ("Full") are also listed in Tables S1–S4 in the Supporting Information.

It can be seen that replacing the bond lengths by their optimized values (the "Angles" approach) has a negligible impact on the calculated RDCs. As the investigated molecules are rather rigid, using the angles to the $z$-axis from the rotated reference structure has no significant impact on most couplings, except for the C3–H3, C4–H4s and C4–H4a couplings in IPC, which are close to the H-bond donor. Thus, the RDCs for the molecules considered can be well described given only the alignment tensor and the reference structure, justifying the analysis in Figure 5.

In Figure 4, we observe some agreement of the RDCs for C1–H1, C3–H3, C4–H4a, $CH_3$–8 and $CH_3$–10 of (−)-IPC with experiment (assuming the determined scaling is accurate). Larger deviations (>10 Hz) occur for C2–H2 and C4–H4s, where the experimental values are similar to (+)-IPC, but the calculated values differ substantially. Both bonds are located near the carbon atom linked to the OH group, capable of forming H-bonds with the alignment medium. Thus, this discrepancy may be caused by an overestimation of the hydrogen bond with PBLG in the force field, which would make the difference between enantiomers more pronounced than in experiment. For (+)-IPC, the agreement is better, but with large differences for C4–H4s and C5–H5. The cylinder approximation matches experiment slightly better than the simulation for (−)-IPC, while the agreement is similar for (+)-IPC.

Higher discrepancies between calculated and experimental RDCs are obtained for quinuclidinol. For both enantiomers, the calculated RDCs do not match the experimental ones, with agreement only due to arbitrary scaling. Interestingly, the RDCs from MD are the closest to the cylinder approximation for *S*-(+)-quinuclidinol after scaling, with a cosine similarity of 0.89 (see Figure S18). This shows that for this specific enantiomer, the alignment by the poses with H-bond is close to the alignment by a cylinder, as the alignment in simulation is dominated by the hydrogen bond (as shown below in Figure 5 and in Figure S18). For the other molecules, this is not the case however.

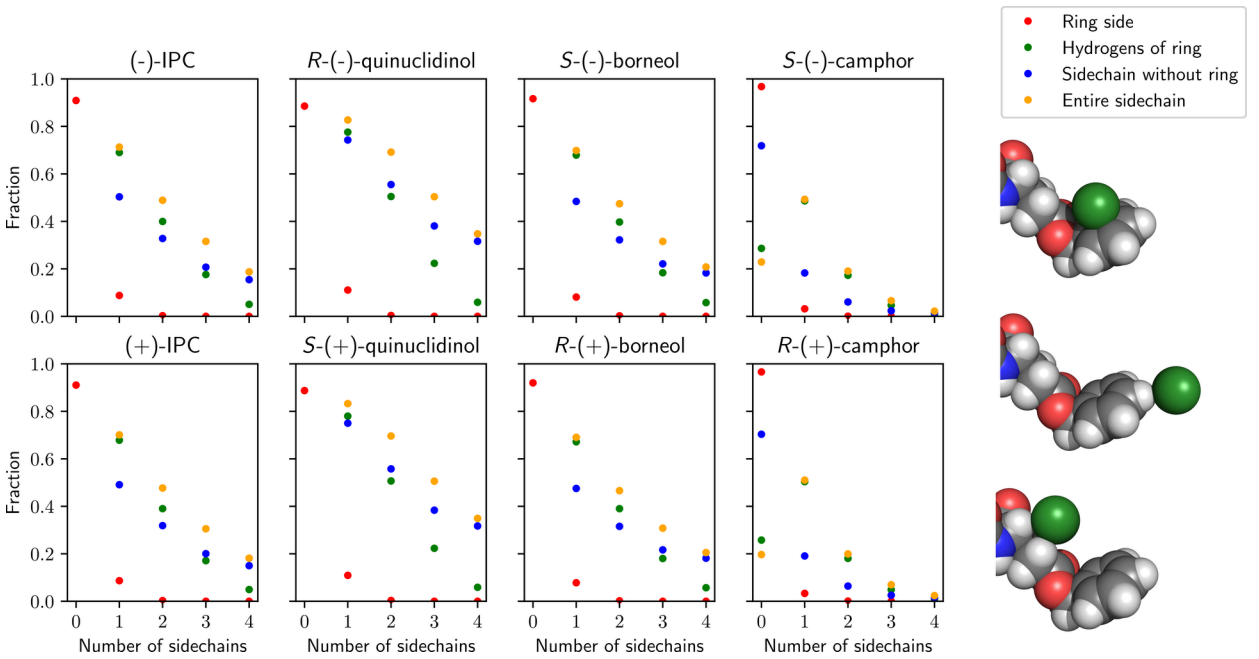


**Figure 6.** Fraction of time the analyte molecule is in contact with different parts of PBLG. The "number of side chains" indicates the number of different repeat units of PBLG, for which the analyte molecule is simultaneously in contact with the respective part. The contact types are depicted on the right, where a single carbon atom in green indicates the analyte molecule. From top to bottom: ring side (near the center of the phenyl ring), hydrogens of ring (near a hydrogen of the phenyl ring), side chain without ring (near the PBLG side chain, excluding the phenyl ring).

For borneol, the agreement is similarly low. As the agreement is not good enough for a proper estimation of the scaling between simulation and experiment, we have found the comparison of the individual RDCs not to be very meaningful. The cylinder approach does not agree with experiment either, but with a smaller deviation.

Even though camphor has no possibility to form the directional noncovalent bonding with PBLG that should, in principle, improve calculated RDCs due to stronger alignment, the RDCs calculated from MDs of enantiomers of this molecule have very good agreement with experimental data. Only the prediction for the $CH_2-6''$, $CH_2-2''$ and $CH_3-11$ couplings is worse (see Figure 4) with deviations around 10–30 Hz. Interestingly, the cylinder approximation does not agree with experiment at all, even though the alignment comes mostly from the nonspecific interaction with the ends of the PBLG side chains, as discussed above and demonstrated in Figure S2.

To compare the orientational distribution of the RDCs and to determine the importance of the interactions considering different fragments of the PBLG side chain, the alignment tensors were fitted to the reference structure of the analyte molecules (see SI) using the RDCs from MD simulations and from experiment. The eigenvectors and eigenvalues of the alignment tensors are demonstrated in Figure 5. Here, the Lambert azimuthal equal-area projection of a semisphere is shown, on which the eigenvectors of the alignment tensors are marked as crosses. The corresponding eigenvalues are indicated by the circles around the eigenvectors, where the line style marks their sign. For example, the alignment tensors of (−)-IPC have good agreement between simulation (black) and experiment (purple): Here, the eigenvectors are close together and the eigenvalues agree in magnitude and sign. In all cases, where hydrogen bonds are present, the eigenvectors of the average over only poses with hydrogen bond agree with the full average, while the magnitude of the eigenvalues is smaller (as the remaining alignment is set to zero).

As mentioned above, the reference structures of a pair of enantiomers are exact point reflections of each other, which allows for a direct comparison between enantiomers. One normalization constant of the eigenvalues was chosen for each pair of enantiomers according to the maximal absolute eigenvalue. The normalization constants of the experimental values and the cylinder prediction were chosen separately, while the one for the full average was also used for the average over the poses with hydrogen bond to the C═O acceptor. Note that partial circles at opposing edges of the semisphere represent the two antipodes of the same eigenvector.

Based on analysis in Figure 5, we have noticed that for IPC, quinuclidinol and borneol, the experimental and simulated alignment tensors differ significantly between enantiomers, while they are by definition identical for the cylindrical prediction. Like the RDCs, the alignment tensors from experiment (purple) and simulation (black) are close for IPC, but disagree for quinuclidinol and borneol. As was observed for the RDCs in Figure 4, the alignment tensors from simulation are almost identical for *S*-(−)- and *R*-(+)-camphor, while the eigenvectors of the fitted alignment tensors from experiment differ slightly. Even though the RDCs agree very well between experiment and simulation, the eigenvectors of the alignment tensors differ noticeably. This indicates that there still is a difference between the two, even though the two different alignment tensors produce similar RDCs for the available couplings.

The alignment tensor average, using only poses with a hydrogen bond with the C═O acceptor in the PBLG side chain, is shown in red for IPC, quinuclidinol and borneol in Figure 5. It is clearly visible that they are very close to the full average in all cases. This again confirms the importance of the

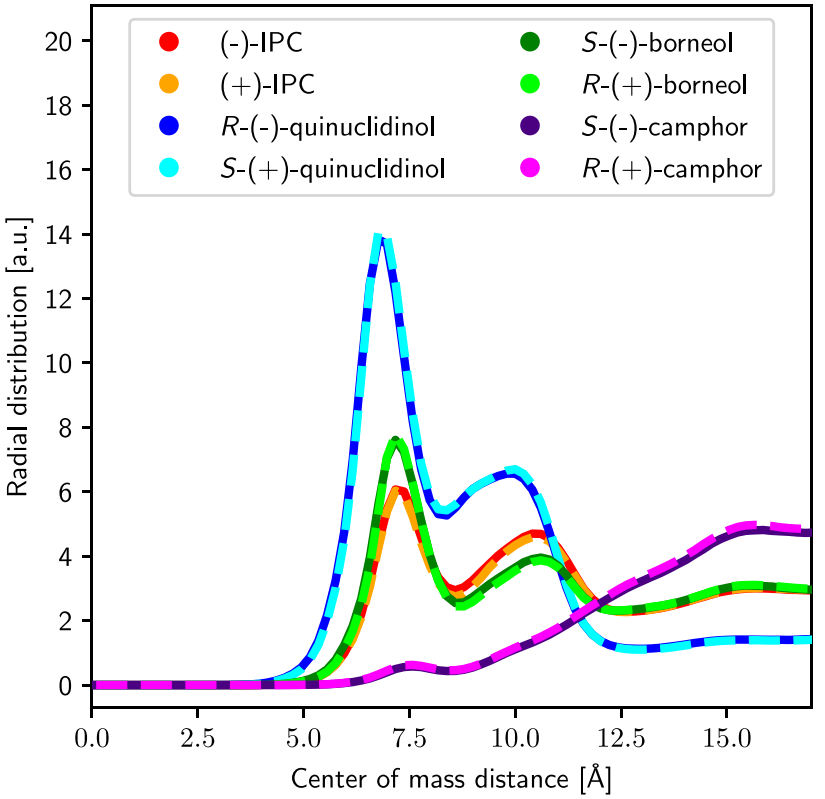


**Figure 7.** Radial distribution of the distance between the center of mass of the analyte molecule and the backbone center of the PBLG chain.

hydrogen bonds for the alignment of the analyte molecules with PBLG.

The above-mentioned PALES prediction, with only steric exclusion by a cylinder, is also shown in cyan in Figure 5. By definition, it is the same for both enantiomers, while the difference between enantiomers comes from the more detailed chiral structure of PBLG. Only for IPC it agrees with experiment to some extend (even though the actual RDCs are determined by the poses with hydrogen bond).

**Mechanism of Alignment and Impact of Hydrogen Bonds.** In Figure 6, the fraction of simulation time, where the analyte molecule is in contact with different parts of the PBLG chain, is demonstrated. The different contact types are depicted on the right side in the figure. A "ring side" contact is defined as an atom of the analyte molecule being within the distance of 3 Å of the carbon atom in the phenyl ring, while a "hydrogen of ring" and "side chain without ring" contacts are defined as an atom $j$ of the analyte molecule being within 1.5 $\sigma_{ij}$ of a ring hydrogen $i$ or nonring side chain atom $i$ of PBLG, respectively. Here, $\sigma_{ij}$ is the Lennard-Jones distance parameter of the AMBER/GAFF force field for the atoms $i$ and $j$. The "number of side chains" is the number of side chains in PBLG for which the analyte molecule is simultaneously in contact with the respective part simultaneously.

IPC and borneol show similar contacts, i.e. mostly via the poses with hydrogen bond to the C═O hydrogen bond acceptor of PBLG, with simultaneous contacts to the ring hydrogens of one or more side chains (in green). From the analysis of the hydrogen bond depicted in Figure S3 and Figure S4 in SI, we clearly see that the O−H ···O H-bond with the C═O acceptor is the most stable and populated H-bond between IPC, quinuclidinol, borneol and the PBLG polymer. Moreover, the highest fraction of H-bonds of this type occur for quinuclidinol with the average lifetime of ∼58 ps, while a slightly lower fraction of H-bonds with lower lifetimes of around 46 ps was found for IPC and borneol (see Figure S5).

For quinuclidinol, the hydrogen bond to PBLG was found to have a higher occurrence during the simulations then for IPC or borneol (see the distribution in Figure S3), and the fraction of multiple side chains being involved is even higher than for the other analytes. If the hydrogen bonds as described in MD are too strong compared to experiment, this may be one of the reasons for lower agreement of RDCs in quinuclidinol compared to the other molecules studied (see below; except for *S*-(−)-borneol). However, the near-perfect similarity of the contacts between enantiomers and between IPC and borneol is notable (see the upper and lower panel in Figure 6). This indicates that their behavior near PBLG is practically identical (i.e., mostly free movements, except for a frequent formation of hydrogen bonds to PBLG for IPC, quinuclidinol and borneol). For the hydrogen bonds, the RDCs differ between the different configurations, while the interaction with PBLG is essentially the same and the hydrogen bond donor is oriented the same way for both enantiomers. The hydrogen bonds formed with the C−O−C acceptor (Figure 3) in PBLG and the interaction with the flat side of the phenyl ring are entirely negligible for the alignment (see Figure 5 and Table S5), because their strength is much weaker compared to the H-bonds with the C═O acceptor.

In Table S6, the largest absolute eigenvalues of the alignment tensor (calculated from eq 4) are shown as a measure of the alignment strength. It includes the full average and the averages of poses having different contacts as explained below. For all molecules, the alignment strength is quite low, meaning that their orientational movement is almost isotropic, despite the frequent hydrogen bond interactions for IPC,

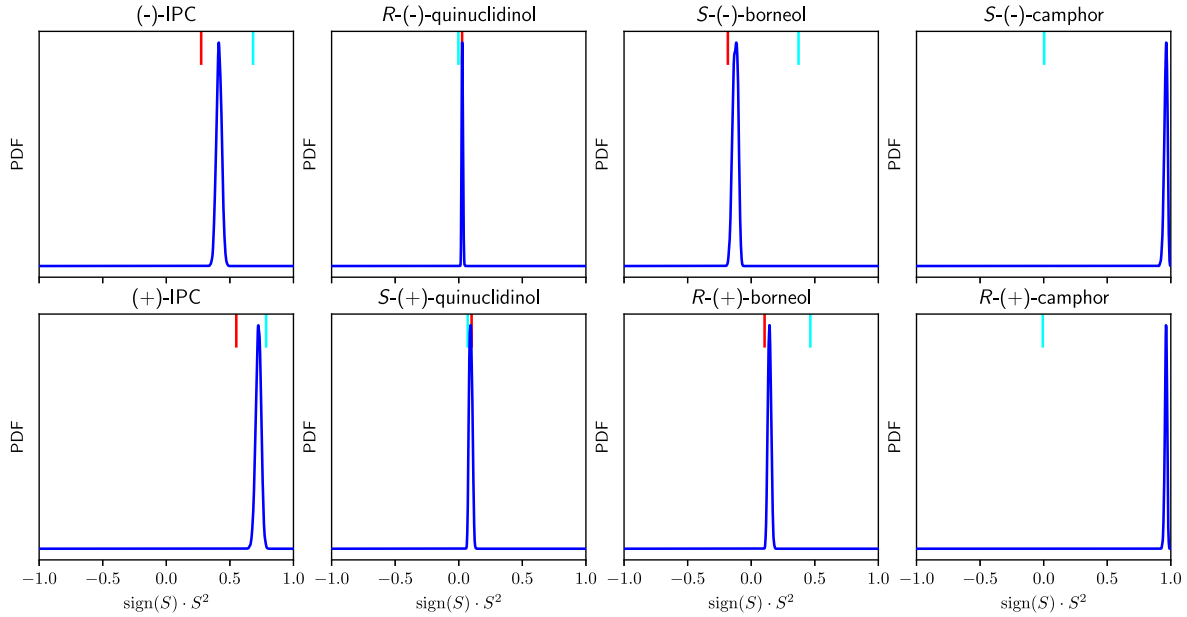


**Figure 8.** Probability distribution function (PDF) of the squared cosine similarity between the calculated and experimental RDCs, considering the statistical uncertainty. The calculated data is the average from MD with a total simulation time of 100 $\mu$s per molecule together with its covariance matrix under the assumption that a Markov chain central limit theorem holds. A value of $S = +1$ indicates perfect agreement, while values near $S = -1$ or even near $S = 0$ mean no agreement. The average of the poses with a hydrogen bond with the C═O acceptor in the PBLG side chain is shown with the red line. The squared cosine similarity between the cylinder (PALES) prediction and is marked with the cyan line.

borneol and quinuclidinol. This can be explained by their spherical nature and that the relevant hydrogen bond acceptors in PBLG are attached to the flexible side chains and do not stay fixed. Notable is that the alignment of *S*-(−)-borneol is significantly lower than for *R*-(+)-borneol. Due to the lack of a hydrogen bond donor for camphor, the interaction with only one (sometimes two) phenyl rings in PBLG occurs and is the most relevant.

From the radial distribution of the distance between the center of mass (COM) of the analyte molecule and the center of the PBLG backbone (approximated by a line determined from the largest principal axis through its center of mass), which is depicted in Figure 7, we observe that the molecules, capable of forming hydrogen bonds with the alignment medium, tend to interact with PBLG on significantly lower distances. At the same time, camphor moves more freely and the alignment takes place further away from the polymer axis. For all molecules though, there is a non-negligible amount of time without contact with PBLG. This suggests that the binding is not very strong and the molecules do not bind for very long, while the contacts and movement are nearly identical between both enantiomers. Our finding agrees with the conclusion reported experimentally by Courtieu et al.[61] and Marxet al.:[42] The analyte molecules do not stay attached to PBLG during the measurement and the difference between the enantiomers is rather small.

The influence of the hydrogen bonds on the RDCs and thus the alignment can also be seen in Figure S2, where the contribution to the RDC average is shown depending on the COM distance to the PBLG center. Here, the largest contributions to the RDCs for camphor are at a larger distance (∼15 Å) than for the other molecules, where there is no hydrogen bond acceptor of PBLG nearby. For the other molecules, the poses with hydrogen bonds are the most important (with the largest contribution at a COM distance between the analyte and PBLG of around ∼7 Å). Somewhat further away, there is again a significant distribution, but often with opposite sign of the RDCs, leading to partial cancellation.

**Comparison to Experiment.** In Figure 8, the predictions obtained from MD simulations are compared to the experimental values from Sager et al.[44] and Marx et al.[42] The two sets of RDCs are compared using the (squared) cosine similarity, as explained in eq 5. To take the statistical uncertainty of the calculated average into account, the predicted RDCs are sampled from a multivariate normal distribution according to the estimated average and its asymptotic covariance matrix. Likewise, the experimental values are sampled from a uniform distribution according to the error estimates. This results in a distribution of cosine similarities which shows the possible range of agreement between the fully converged simulation and the ”true” values from experiment. The value for the average using only the poses with hydrogen bond to the C═O acceptor is demonstrated by the red lines in Figure 8. Its agreement with the experimental data is very close to the full MD average (shown in blue).

For IPC, the similarity to experiment depends on the enantiomer: While (+)-IPC has almost perfect agreement, the cosine similarity is somewhat lower (but still clearly positive) for (−)-IPC. For quinuclidinol and borneol, the similarity is close to 0, meaning that the prediction does not match experiment. For camphor, the cosine similarity with experiment is also very close to +1 for both enantiomers. As shown above in Figure 4, the agreement for the PALES model is generally lower.

In all cases, the simulation time was long enough such that the model (based on an all-atom force field) and the experimental data can be compared conclusively, i.e. without being affected by statistical uncertainty. Still, for a comparison between the calculated and experimental values, the alignment

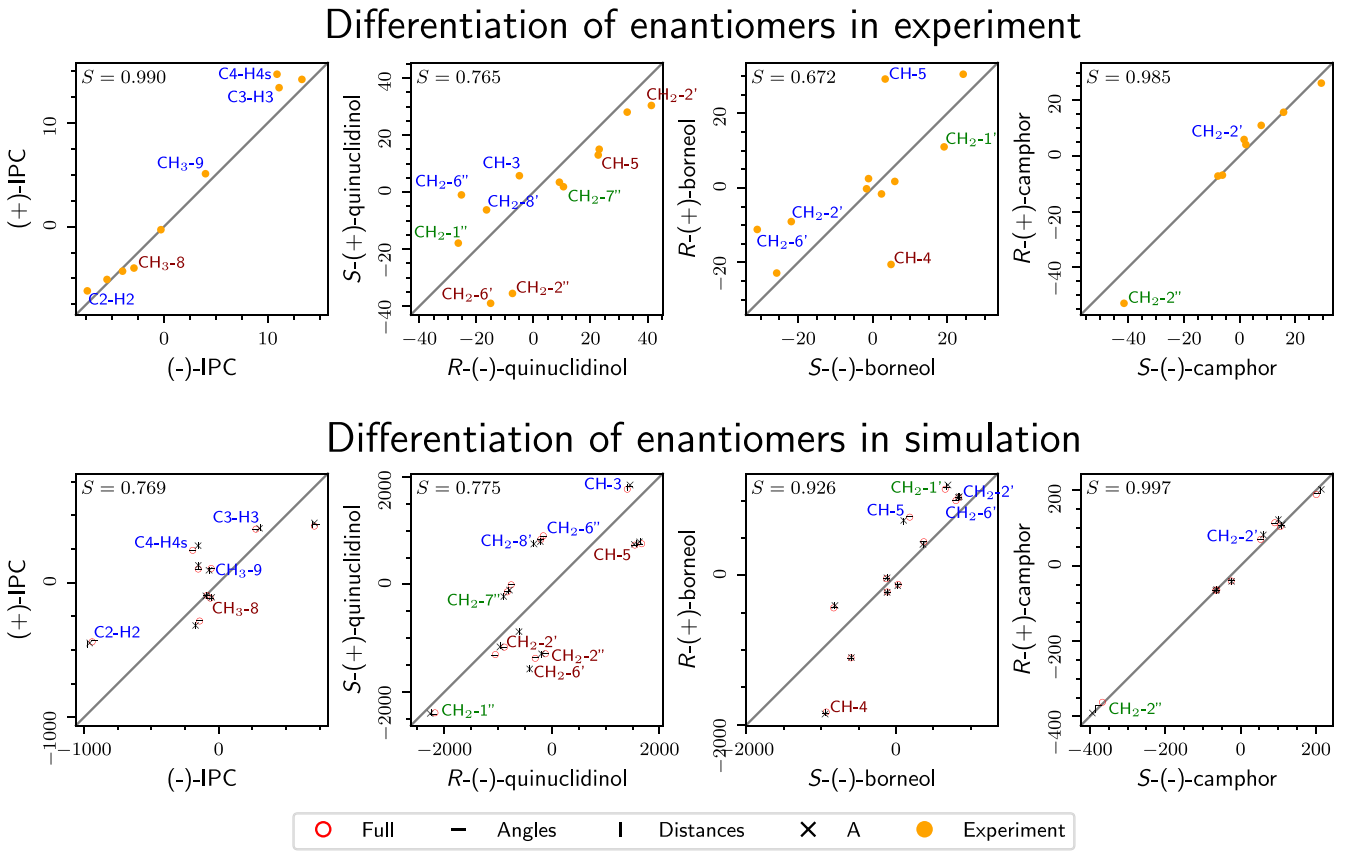


**Figure 9.** Comparison of the RDCs ($2D_{ij}$) in Hz between pairs of enantiomers from experiment (plots in the upper panel) and simulation (plots in the lower panel). No scaling for the calculated RDCs (in comparison to the data in Figure 4) was applied. The couplings with the largest deviations between enantiomers in experiment are labeled. Here, blue indicates that the difference between enantiomers is positive for both experiment and simulation; red indicates that it is negative for both and green that its sign differs. The cosine similarity between the RDCs of the enantiomers (using the calculated RDCs from the "Full" approach, see Figure 4 and the text) is shown in the respective top left corner.

tensor is not conclusive in some cases. As an example, the agreement is good for both *S*-(−)-camphor and *R*-(+)-camphor, when comparing the RDCs directly (Figure 8), even though the fitted alignment tensors differ substantially from the experimental ones (Figure 5). This can be explained by the low number of distinct RDCs (see Figure 4) used for the experimental fit.

Figure 9 is a comparison of the RDC values between enantiomers both for the experimentally measured data and the RDCs calculated with the MD simulations (which are also shown in Figure 4). Note that here, the constant scaling was not applied, such that the calculated values are much larger in magnitude due to the small simulation box compared to the relatively low PBLG concentration in experiment. The cosine similarity between enantiomers is similarly low for quinuclidinol (0.765/0.775) and borneol (0.672/0.926) and very high for camphor (0.985/0.997) both in experiment and simulation, respectively. For IPC however, it is much lower in simulation (0.769) compared to experiment (0.990), as the RDCs for (+)-IPC differ more as shown in Figure 4. The couplings with the largest deviations between enantiomers in experiment (> ∼ 30% of the largest absolute deviation), are marked by their names in both rows of Figure 9.

To validate whether we can confirm the experimental difference between enantiomers via MD simulations, we compare the sign of the deviations for the marked couplings: For IPC, all marked deviations have the same sign; for quinuclidinol, all except $CH_2$−1″ and $CH_2$−7″; and for borneol, all except $CH_2$−1′. For camphor, the RDCs between enantiomers are very close both in experiment and simulation, making a differentiation unfeasible. This is evidence that the simulation scheme applied in this study permits the distinction of the alignment of the enantiomers with a qualitative correspondence to experimental data.

**Model Verification.** To confirm the quality of the computational approach, where a single analyte molecule and a single PBLG chain were considered in the MD simulations, we performed additional MD simulations for 15 $\mu$s, where 8 analyte molecules were present in the simulation box. In addition, simulations both with one PBLG and two PBLG chains in the box were done. For the latter, the box size in the xy-plane was changed to ∼4.4 nm.

The results are depicted in the SI, with a comparison of the RDCs calculated for different systems considered in Figures S15−S22. Comparing the RDCs between the simulations with one and with eight analyte molecules, we have detected small changes in the RDC values. This is caused by interactions between the analyte molecules in the solvent environment. However, the cosine similarity of the RDCs calculated with one or eight analyte molecules is 0.93 for (−)-IPC, 0.95 for (+)-IPC, 0.98 for *R*-(−)-quinuclidinol, 0.96 for *S*-(+)-quinuclidinol, and ≥0.99 for borneol and camphor. Thus, the consideration of multiple molecules in the performed simulations does not change the applicability for enantiodiscrimination. The use of two PBLG chains in the PBC box has

been found to matter even less, resulting in a cosine similarity of ∼1.00 in all cases.

Since our report considers the explicit solvent effects in the RDC calculations for the first time, allowing for an appropriate comparison to RDCs obtained experimentally, we also checked its impact by doing MD simulations in the gas phase using Langevin dynamics[95] with an inverse friction constant of 2 ps instead of the thermostat and without pressure coupling. We have found that the analytes stayed always very close to the PBLG chain, leading to different orientations and in most cases, we observed large differences to the RDCs calculated with explicit chloroform and worse agreement with experiment.

**Discussion.** We demonstrated the application of classical molecular dynamics simulations with explicit solvent for the prediction of residual dipolar couplings in both enantiomers of four chiral, almost spherical molecules aligned by PBLG in chloroform. Since RDCs may, in principle, be used for the determination of the absolute configuration of chiral molecules and the nearly spherical molecules considered here show rather small alignment with small differences between enantiomers, significant attention has been put on the proper convergence of the RDC calculations, which was verified by their estimated statistical uncertainty. We have found that in order to achieve sufficient sampling, simulations with a length of tens of microseconds are necessary depending on the analyte molecule. To achieve this, 1000 parallel MD simulations were performed using an automated workflow, resulting in a total of 100 $\mu$s long MD runs for each enantiomer involved. Using the MD trajectories, the RDC couplings and alignment tensors were calculated and compared to experimental NMR data.

While the MD simulations were performed with a large computational effort and high statistical certainty, there are several possible fundamental limitations of the model: First, the accuracy of the force field could play a role: The alignment depends on the average over all possible poses between analyte molecule and alignment medium. Therefore, the accurate consideration of electrostatic interactions and hydrogen bonds plays a central role, but were only described by point charges in this work. Such a treatment was found to have limited accuracy for hydrogen bonds.[96] Simulations using polarizable force fields or further force field improvements are worth to be considered, however, they are beyond the scope of the present investigation.

Second, only a pure chloroform solution was modeled in the simulations, while a contamination with water in experiment cannot be entirely excluded, as the water can bind at the interface of the analyte to the alignment medium, resulting experimentally in peak broadening and sometimes even undetectable NMR signals. Moreover, water most likely will impact the hydrogen bond interaction patterns between solutes and alignment medium.[97] In the present study, we demonstrate the critical importance of H-bonds for the alignment of the analyte molecules. Therefore, subtle disruptions may impact experimentally estimated couplings, also considering the close to spherical shape of all molecules in this study. As no information about the water content of samples is known, the importance of water is particularly difficult to judge at this point.

Finally, the PBLG model used represents a single polymer strand of infinite length. It is an approximation of the "real" liquid crystalline phase, which may be not identical to experimental conditions. The ends of PBLG might be charged and cause significant contact times of the solute molecule. Since the structure of such ends in chloroform is unknown and their influence on the RDCs (if any) would depend on the concentration and molecular weight of the synthesized polymer chains, this effect could clearly not be taken into account in the PBLG model used here. However, we estimate from previous and current results that the used model represents the major component responsible for aligning solute molecules.

A comparison with experimental data shows different agreement for the different molecules. For camphor, which does not have an H-bond donor, the agreement is almost perfect and the difference between enantiomers is also very small. Equally, the agreement for (+)-IPC is good (cosine similarity 0.85) and still present for (−)-IPC (cosine similarity 0.64). However, for both enantiomers of borneol and quinuclidinol, the results show larger deviations from experiment. Assuming validity of experimental data, it is apparent that in all cases with deviations, significant H-bond formation is involved. Even more, the resulting predicted RDCs are essentially the same if only poses with H-bond formation are considered, proving the dominance of this interaction for alignment. In simulation, H-bonds between PBLG and IPC, quinuclidinol and borneol are predominantly found to be with a length of ca. 1.6−1.7 Å and an angle of ca. 165−170 degrees. Such structural parameters are characteristic for rather stable H-bonds, which we found to be critically important for the alignment. In fact, the alignment can be almost completely explained by the poses with hydrogen bond to the C═O acceptor in the PBLG side chain, while the hydrogen bond to the C−O−C acceptor is irrelevant to the alignment in all cases. Furthermore, it is evident that besides the H-bond formation, the simultaneous interaction with the phenyl rings of (neighboring) side chains is important, with the latter making contact to the analyte molecule in more than ∼80% of the simulation time. The alignment of camphor also appears to be mainly determined via contacts to phenyl rings, although no hydrogen bonds are formed and exceptionally good agreement with experiment could be reached.

Although measured and predicted RDCs deviate stronger for the analytes with H-bond donors, similar trends in the relative changes of calculated RDCs (in comparison to experimental ones) between enantiomers could be observed for all molecules studied. This observation demonstrates evidence that the differences for enantiomers, measured experimentally, are indeed included in the presented interaction model. The differential alignment of enantiomers behaves the same *in silico* as in the experiment, as characterized by the hydrogen bond properties[44] and their contacts with different parts of the PBLG side chains. Here, the approach described in Gouilleux et al.[86] could provide additional experimental evidence from NMR measurements.

A comparison with the established cylindrical PALES approach, which shows considerably worse agreement with experiment, indicates that molecular modeling with atomistic resolution is necessary and shows a real potential for further RDC predictions toward the determination of the absolute configuration of chiral molecules. It also fails for quinuclidinol and borneol, where the agreement of our simulations is poor as well. Surprisingly, even for camphor PALES does not agree with experiment, although it lacks an H-bond donor, i.e. there is no immediate directionality and bonding preference during

alignment. Here, the atomistic interactions with the phenyl ring of the PBLG side chains play a major role and thus, the method developed here advances the current state-of-the-art.

Additionally, we demonstrate that RDCs can be sufficiently described by an average over the orientation of the analyte molecules we considered; they are rigid enough that their internal motion can be neglected with the exception of the fast rotating $CH_3$ groups, for which the pseudo-RDC in the direction of the bond to the neighboring heavy atom can be used instead of explicit averaging. The consideration of multiple analyte molecules in the simulation box demonstrated slight changes in the RDC values with rather low impact on the final cosine similarities in comparison to experiment. There was virtually no difference if one or two PBLG chains are included in the simulation, indicating a well-designed theoretical model for the RDCs estimation.

## CONCLUSIONS

In this study, we report and investigate the effectiveness of MD simulations for the calculation of RDCs in analyte molecules aligned by a PBLG-based mesophase. Our results show that the prediction of RDCs is indeed feasible and that differences between enantiomers can be observed. In almost all studied cases, the sign of the relative size of differences in RDCs between enantiomers is represented correctly, although significant differences to individual experimental RDCs do exist. This might be partially explained by force field limitations, a possible sample contamination with water or interactions with the (possibly charged) ends of the PBLG molecules in experiment. At the same time, we found that the inclusion of multiple analyte molecules or PBLG chains in the simulations did not change the RDCs significantly and thus, the exact setup of the simulation box does not explain the observed discrepancies. Additionally, an imperfect alignment to the magnetic field of the PBLG helices should only scale the RDCs by a constant factor. Also predicting the correct scaling of the RDCs, which requires taking into account the PBLG concentration and their average alignment to the magnetic field, as well as a very accurate representation of the binding of the analyte molecules to PBLG, is still challenging. It should be noted that the molecules studied here all possess almost spherical shape, which makes the accurate prediction of alignment particularly difficult.

A detailed study of obtained trajectories revealed that the interactions with PBLG are nearly identical for the pairs of enantiomers and the difference in alignment is due to the different orientation during these interaction, not because the interactions differ. For the molecules with hydrogen bond donor, the interaction with PBLG is dominated by the hydrogen bond. This is most clearly demonstrated by comparing the behavior of borneol and camphor, where most of the interaction with PBLG takes place much closer for the former even though they only differ by the functional group.

Overall, RDCs differ more significantly between enantiomers for IPC, quinuclidinol and borneol, which possess H-bond donor groups, due to the different absolute configuration when forming a hydrogen bond with PBLG. This is in contrast to camphor, where the lack of hydrogen bonding leads to very similar RDCs for the enantiomers in both experiment and simulation.

As such, we have provided new insights for the simulation of PBLG-based mesophases and that it is possible to calculate the alignment of different enantiomers using MD simulations in sufficient detail that the determination of absolute configuration seems, in principle, conceivable. However, the prediction of individual RDCs still has deviations with ample room for improvement due to the complex dynamics of the polymer's side chains and their interactions with the analyte molecules in a real sample. A very important point seems to be the accurate representation of H-bonds, for which the force field representation as electrostatic point charges used here may not be sufficient and the use of a correction or a polarizable force field should be investigated. Regarding the positive trends and possible further improvement of predictions, we are confident that RDCs together with MD simulations of differential alignment of enantiomeric pairs will enable the determination of absolute configuration without chemical modification of analyte molecules in the future.

## AUTHOR INFORMATION


### Corresponding Author

**Mariana Kozlowska** − *Institute of Nanotechnology, Karlsruhe Institute of Technology (KIT), 76131 Karlsruhe, Germany;* orcid.org/0000-0001-8471-8914; Email: mariana.kozlowska@kit.edu

### Authors

**David Elsing** − *Institute of Nanotechnology, Karlsruhe Institute of Technology (KIT), 76131 Karlsruhe, Germany*

**Burkhard Luy** − *Institute for Biological Interfaces 4 and Institute of Organic Chemistry, Karlsruhe Institute of Technology (KIT), 76131 Karlsruhe, Germany;* orcid.org/0000-0001-9580-6397


### Author Contributions

Conceptualization: D.E., B.L., M.K.; methodology: D.E., B.L., M.K.; software: D.E.; validation: D.E.; formal analysis: D.E.; investigation: D.E.; data curation: D.E.; writing - original draft: D.E.; writing - review and editing: D.E., B.L., M.K; visualization: D.E.; resources: M.K.; supervision: B.L., M.K.; project administration: M.K.; funding acquisition: B.L., M.K.

### Notes

The authors declare no competing financial interest.

## ACKNOWLEDGMENTS


This research was funded by the Joint Lab "Virtual Materials Design" and VirtMat initiative within the Helmholtz Research Field "Information" (43.35.02). MK acknowledges funding from the Deutsche Forschungsgemeinschaft (DFG) via the GRK 2450 "Scale bridging methods of computational nano-

science". This work was performed on the HoreKa supercomputer funded by the Ministry of Science, Research and the Arts Baden-Württemberg and by the Federal Ministry of Education and Research. The authors thank Henrik Schopmans and Montserrat Penaloza Amion for the discussion on the calculation of RDCs by simulation methods.

## REFERENCES

(1) Bijvoet, J. M.; Peerdeman, A. F.; van Bommel, A. J. Determination of the Absolute Configuration of Optically Active Compounds by Means of X-Rays. *Nature* **1951**, *168*, 271−272.
(2) Flack, H. D.; Bernardinelli, G. The use of X-ray crystallography to determine absolute configuration. *Chirality* **2008**, *20*, 681−690.
(3) Berova, N.; Nakanishi, K.; Woody, R. W. *Circular dichroism: principles and applications*; John Wiley & Sons, 2000.
(4) Cianciosi, S. J.; Spencer, K. M.; Freedman, T. B.; Nafie, L. A.; Baldwin, J. E. Synthesis and gas-phase vibrational circular dichroism of (+)-(S,S)-cyclopropane-1,2−2H2. *J. Am. Chem. Soc.* **1989**, *111*, 1913−1915.
(5) Patterson, D.; Schnell, M. New studies on molecular chirality in the gas phase: enantiomer differentiation and determination of enantiomeric excess. *Phys. Chem. Chem. Phys.* **2014**, *16*, 11114−11123.
(6) Dale, J. A.; Mosher, H. S. Nuclear magnetic resonance enantiomer regents. Configurational correlations via nuclear magnetic resonance chemical shifts of diastereomeric mandelate, O-methylmandelate, and $\alpha$-methoxy-$\alpha$-trifluoromethylphenylacetate (MTPA) esters. *J. Am. Chem. Soc.* **1973**, *95*, 512−519.
(7) Kong, L.-Y.; Wang, P. Determination of the absolute configuration of natural products. *Chin. J. Nat. Med.* **2013**, *11*, 193−198.
(8) Pereda-Miranda, R.; Bautista, E.; Martínez-Fructuoso, L.; Fragoso-Serrano, M. From Relative to Absolute Stereochemistry of Secondary Metabolites: Applications in Plant Chemistry. *Rev. Bras. Farmacogn.* **2023**, *33*, 1−48.
(9) Saupe, A.; Englert, G. High-Resolution Nuclear Magnetic Resonance Spectra of Orientated Molecules. *Phys. Rev. Lett.* **1963**, *11*, 462−464.
(10) Saupe, A. Kernresonanzen in kristallinen Flüssigkeiten und in kristallinflüssigen Lösungen. *Teil I. Zeitschrift für Naturforschung A* **1964**, *19*, 161−171.
(11) Böttcher, B.; Thiele, C. M. *eMagRes.*; John Wiley & Sons, Ltd, 2012; Vol. *1*; pp 169−180.
(12) Kummerlöwe, G.; Luy, B. Residual dipolar couplings as a tool in determining the structure of organic molecules. *TrAC, Trends Anal. Chem.* **2009**, *28*, 483−493.
(13) Schuetz, A.; Junker, J.; Leonov, A.; Lange, O. F.; Molinski, T. F.; Griesinger, C. Stereochemistry of Sagittamide A from Residual Dipolar Coupling Enhanced NMR. *J. Am. Chem. Soc.* **2007**, *129*, 15114−15115.
(14) Troche-Pesqueira, E.; Anklin, C.; Gil, R. R.; Navarro-Vázquez, A. Computer-Assisted 3D Structure Elucidation of Natural Products using Residual Dipolar Couplings. *Angew. Chem., Int. Ed.* **2017**, *56*, 3660−3664.
(15) Tzvetkova, P.; Sternberg, U.; Gloge, T.; Navarro-Vázquez, A.; Luy, B. Configuration determination by residual dipolar couplings: accessing the full conformational space by molecular dynamics with tensorial constraints. *Chem. Sci.* **2019**, *10*, 8774−8791.
(16) Ibáñez de Opakua, A.; Klama, F.; Ndukwe, I. E.; Martin, G. E.; Williamson, R. T.; Zweckstetter, M. Determination of Complex Small-Molecule Structures Using Molecular Alignment Simulation. *Angew. Chem., Int. Ed.* **2020**, *59*, 6172−6176.
(17) Thiele, C. M.; Marx, A.; Berger, R.; Fischer, J.; Biel, M.; Giannis, A. Determination of the Relative Configuration of a Five-Membered Lactone from Residual Dipolar Couplings. *Angew. Chem., Int. Ed.* **2006**, *45*, 4455−4460.
(18) Thiele, C. M.; Maliniak, A.; Stevensson, B. Use of Local Alignment Tensors for the Determination of Relative Configurations in Organic Compounds. *J. Am. Chem. Soc.* **2009**, *131*, 12878−12879.
(19) Nath, N.; d'Auvergne, E. J.; C, Griesinger Long-Range Residual Dipolar Couplings: A Tool for Determining the Configuration of Small Molecules. *Angew. Chem., Int. Ed.* **2015**, *54*, 12706−12710.
(20) Sackmann, E.; Meiboom, S.; Snyder, L. C. Relation of nematic to cholesteric mesophases. *J. Am. Chem. Soc.* **1967**, *89*, 5981−5982.
(21) Sackmann, E.; Meiboom, S.; Snyder, L. C. Nuclear magnetic resonance spectra of enantiomers in optically active liquid crystals. *J. Am. Chem. Soc.* **1968**, *90*, 2183−2184.
(22) Berger, R.; Courtieu, J.; Gil, R. R.; Griesinger, C.; Köck, M.; Lesot, P.; Luy, B.; Merlet, D.; Navarro-Vázquez, A.; Reggelin, M.; et al. Is Enantiomer Assignment Possible by NMR Spectroscopy Using Residual Dipolar Couplings from Chiral Nonracemic Alignment Media?−A Critical Assessment. *Angew. Chem., Int. Ed.* **2012**, *51*, 8388−8391.
(23) Farjon, J.; Merlet, D.; Lesot, P.; Courtieu, J. Enantiomeric excess measurements in weakly oriented chiral liquid crystal solvents through 2D 1H selective refocusing experiments. *J. Magn. Reson.* **2002**, *158*, 169−172.
(24) Ziani, L.; Lesot, P.; Meddour, A.; Courtieu, J. Empirical determination of the absolute configuration of small chiral molecules using natural abundance 2H NMR in chiral liquid crystals. *Chem. Commun.* **2007**, 4737−4739.
(25) Kummerlöwe, G.; Schmitt, S.; Luy, B. Cross-Fitting of Residual Dipolar Couplings. *Open Spectrosc. J.* **2010**, *4*, 16−27.
(26) Hus, J.-C.; Marion, D.; Blackledge, M. Determination of Protein Backbone Structure Using Only Residual Dipolar Couplings. *J. Am. Chem. Soc.* **2001**, *123*, 1541−1542.
(27) Bax, A. Weak alignment offers new NMR opportunities to study protein structure and dynamics. *Protein Sci.* **2003**, *12*, 1−16.
(28) Dosset, P.; Hus, J.-C.; Marion, D.; Blackledge, M. A novel interactive tool for rigid-body modeling of multi-domain macromolecules using residual dipolar couplings. *J. Biomol. NMR* **2001**, *20*, 223−231.
(29) Zweckstetter, M.; Hummer, G.; Bax, A. Prediction of Charge-Induced Molecular Alignment of Biomolecules Dissolved in Dilute Liquid-Crystalline Phases. *Biophys. J.* **2004**, *86*, 3444−3460.
(30) Zweckstetter, M. NMR: prediction of molecular alignment from structure using the PALES software. *Nat. Protoc.* **2008**, *3*, 679−690.
(31) Azurmendi, H. F.; Bush, C. A. Tracking Alignment from the Moment of Inertia Tensor (TRAMITE) of Biomolecules in Neutral Dilute Liquid Crystal Solutions. *J. Am. Chem. Soc.* **2002**, *124*, 2426−2427.
(32) Almond, A.; Axelsen, J. B. Physical Interpretation of Residual Dipolar Couplings in Neutral Aligned Media. *J. Am. Chem. Soc.* **2002**, *124*, 9986−9987.
(33) Wu, B.; Petersen, M.; Girard, F.; Tessari, M.; Wijmenga, S. S. Prediction of molecular alignment of nucleic acids in aligned media. *J. Biomol. NMR* **2006**, *35*, 103−115.
(34) Ibáñez de Opakua, A.; Zweckstetter, M. Extending the applicability of P3D for structure determination of small molecules. *Magn. Reson.* **2021**, *2*, 105−116.
(35) Aroulanda, C.; Lesot, P. Molecular enantiodiscrimination by NMR spectroscopy in chiral oriented systems: Concept, tools, and applications. *Chirality* **2022**, *34*, 182−244.
(36) Pizzirusso, A.; Di Cicco, M. B.; Tiberio, G.; Muccioli, L.; Berardi, R.; Zannoni, C. Alignment of Small Organic Solutes in a Nematic Solvent: The Effect of Electrostatic Interactions. *J. Phys. Chem. B* **2012**, *116*, 3760−3771.
(37) Frank, A. O.; Freudenberger, J. C.; Shaytan, A. K.; Kessler, H.; Luy, B. Direct prediction of residual dipolar couplings of small molecules in a stretched gel by stochastic molecular dynamics simulations. *Magn. Reson. Chem.* **2015**, *53*, 213−217.
(38) Canet, I.; Courtieu, J.; Loewenstein, A.; Meddour, A.; Pechine, J. M. Enantiomeric analysis in a polypeptide lyotropic liquid crystal by deuterium NMR. *J. Am. Chem. Soc.* **1995**, *117*, 6520−6526.

(39) Aroulanda, C.; Sarfati, M.; Courtieu, J.; Lesot, P. Investigation of the enantioselectivity of three polypeptide liquid-crystalline solvents using NMR spectroscopy. *Enantiomer* **2001**, *6*, 281−287.
(40) Luy, B.; Kobzar, K.; Kessler, H. An Easy and Scalable Method for the Partial Alignment of Organic Molecules for Measuring Residual Dipolar Couplings. *Angew. Chem., Int. Ed.* **2004**, *43*, 1092−1094.
(41) Luy, B. Disinction of enantiomers by NMR spectroscopy using chiral orienting media. *J. Indian Inst. Sci.* **2010**, *90*, 119−132.
(42) Marx, A.; Schmidts, V.; Thiele, C. M. How different are diastereomorphous orientations of enantiomers in the liquid crystalline phases of PBLG and PBDG: a case study. *Magn. Reson. Chem.* **2009**, *47*, 734−740.
(43) Lesot, P.; Aroulanda, C.; Berdagué, P.; Meddour, A.; Merlet, D.; Farjon, J.; Giraud, N.; Lafon, O. Multinuclear NMR in polypeptide liquid crystals: Three fertile decades of methodological developments and analytical challenges. *Prog. Nucl. Magn. Reson. Spectrosc.* **2020**, *116*, 85−154.
(44) Sager, E.; Tzvetkova, P.; Lingel, A.; Gossert, A. D.; Luy, B. Hydrogen bond formation may enhance RDC-based discrimination of enantiomers. *Magn. Reson. Chem.* **2024**, DOI: 10.1002/mrc.5448.
(45) Sager, E. Residual dipolar couplings: a complementary tool for stereochemistry determination of drug compounds. Ph.D. thesis, Karlsruher Institut für Technologie (KIT), 2019.
(46) Tolman, J. R. A Novel Approach to the Retrieval of Structural and Dynamic Information from Residual Dipolar Couplings Using Several Oriented Media in Biomolecular NMR Spectroscopy. *J. Am. Chem. Soc.* **2002**, *124*, 12020−12030.
(47) Levitt, M. H. *Spin Dynamics: Basics of Nuclear Magnetic Resonance*; John Wiley & Sons, 2013.
(48) Krugh, T. R.; Bernheim, R. A. Anisotropies and Absolute Signs of the Indirect SpinSpin Coupling Constants in $^{13}CH_3F$. *J. Chem. Phys.* **1970**, *52*, 4942−4949.
(49) Kramer, F.; Deshmukh, M. V.; Kessler, H.; Glaser, S. J. Residual dipolar coupling constants: An elementary derivation of key equations. *Concepts Magn. Reson., Part A* **2004**, *21A*, 10−21.
(50) Burnell, E.; de Lange, C. Effects of interaction between molecular internal motion and reorientation on NMR of anisotropic liquids. *J. Magn. Reson. (1969−1992)* **1980**, *39*, 461−480.
(51) Losonczi, J. A.; Andrec, M.; Fischer, M. W.; Prestegard, J. H. Order Matrix Analysis of Residual Dipolar Couplings Using Singular Value Decomposition. *J. Magn. Reson.* **1999**, *138*, 334−342.
(52) Stephens, P. J.; Devlin, F. J.; Chabalowski, C. F.; Frisch, M. J. Ab Initio Calculation of Vibrational Absorption and Circular Dichroism Spectra Using Density Functional Force Fields. *J. Phys. Chem.* **1994**, *98*, 11623−11627.
(53) Schäfer, A.; Horn, H.; Ahlrichs, R. Fully optimized contracted Gaussian basis sets for atoms Li to Kr. *J. Chem. Phys.* **1992**, *97*, 2571−2577.
(54) Sun, Q.; Zhang, X.; Banerjee, S.; Bao, P.; Barbry, M.; Blunt, N. S.; Bogdanov, N. A.; Booth, G. H.; Chen, J.; Cui, Z.-H.; et al. Recent developments in the PySCF program package. *J. Chem. Phys.* **2020**, *153*, 024109.
(55) Enthart, A.; Freudenberger, J. C.; Furrer, J.; Kessler, H.; Luy, B. The CLIP/CLAP-HSQC: Pure absorptive spectra for the measurement of one-bond couplings. *J. Magn. Reson.* **2008**, *192*, 314−322.
(56) Tzvetkova, P.; Simova, S.; Luy, B. P. E. HSQC: A simple experiment for simultaneous and sign-sensitive measurement of (1JCH+DCH) and (2JHH+DHH) couplings. *J. Magn. Reson.* **2007**, *186*, 193−200.
(57) Naumann, C.; Bubb, W. A.; Chapman, B. E.; Kuchel, P. W. Tunable-Alignment Chiral System Based on Gelatin for NMR Spectroscopy. *J. Am. Chem. Soc.* **2007**, *129*, 5340−5341.
(58) Wang, H.; Eberstadt, M.; Olejniczak, E. T.; Meadows, R. P.; Fesik, S. W. A liquid crystalline medium for measuring residual dipolar couplings over a wide range of temperatures. *J. Biomol. NMR* **1998**, *12*, 443−446.
(59) Marx, A.; Thiele, C. Orientational Properties of Poly-$\gamma$-benzyl-L-glutamate: Influence of Molecular Weight and Solvent on Order Parameters of the Solute. *Chem. - Eur. J.* **2009**, *15*, 254−260.
(60) Sinnaeve, D.; Ilgen, J.; Di Pietro, M. E.; Primozic, J. J.; Schmidts, V.; Thiele, C. M.; Luy, B. Probing Long-Range Anisotropic Interactions: a General and Sign-Sensitive Strategy to Measure 1H-1H Residual Dipolar Couplings as a Key Advance for Organic Structure Determination. *Angew. Chem., Int. Ed.* **2020**, *59*, 5316−5320.
(61) Courtieu, J.; Aroulanda, C.; Lesot, P.; Meddour, A.; Merlet, D. Evolution of the Saupe order parameters of enantiomers from a racemic to a non-racemic liquid crystal solvent: an original light on the absolute configuration determination problem. *Liq. Cryst.* **2010**, *37*, 903−912.
(62) Helfrich, J.; Hentschke, R.; Apel, U. M. Molecular dynamics simulation study of poly(.gamma.-benzyl L-glutamate) in dimethylformamide. *Macromolecules* **1994**, *27*, 472−482.
(63) Helfrich, J.; Hentschke, R. Molecular Dynamics Simulation of Macromolecular Interactions in Solution: Poly(.gamma.-benzyl glutamate) in Dimethylformamide and Tetrahydrofuran. *Macromolecules* **1995**, *28*, 3831−3841.
(64) Ekström, U.; Visscher, L.; Bast, R.; Thorvaldsen, A. J.; Ruud, K. Arbitrary-Order Density Functional Response Theory from Automatic Differentiation. *J. Chem. Theory Comput.* **2010**, *6*, 1971−1980.
(65) Wang, L.-P.; Song, C. Geometry optimization made simple with translation and rotation coordinates. *J. Chem. Phys.* **2016**, *144*, 214108.
(66) Arnott, S.; Dover, S. D. Refinement of bond angles of an $\alpha$-helix. *J. Mol. Biol.* **1967**, *30*, 209−212.
(67) Bamford, C. H.; Hanby, W.; Happey, F. The structure of synthetic polypeptides I. X-ray investigation. *Proc. R. Soc. London, Ser. A* **1951**, *205*, 30−47.
(68) RDKit: Open-source cheminformatics. https://www.rdkit.org, Version 2022.03.2.
(69) Cornell, W. D.; Cieplak, P.; Bayly, C. I.; Kollman, P. A. Application of RESP charges to calculate conformational energies, hydrogen bond energies, and free energies of solvation. *J. Am. Chem. Soc.* **1993**, *115*, 9620−9631.
(70) Ditchfield, R.; Hehre, W. J.; Pople, J. A. Self-Consistent Molecular-Orbital Methods. IX. An Extended Gaussian-Type Basis for Molecular-Orbital Studies of Organic Molecules. *J. Chem. Phys.* **1971**, *54*, 724−728.
(71) Hariharan, P. C.; Pople, J. A. The influence of polarization functions on molecular orbital hydrogenation energies. *Theor. Chim. Acta* **1973**, *28*, 213−222.
(72) Hehre, W. J.; Ditchfield, R.; Pople, J. A. SelfConsistent Molecular Orbital Methods. XII. Further Extensions of GaussianType Basis Sets for Use in Molecular Orbital Studies of Organic Molecules. *J. Chem. Phys.* **1972**, *56*, 2257−2261.
(73) Case, D. A.; Aktulga, H. M.; Belfon, K.; Ben-Shalom, I. Y.; Brozell, S. R.; Cerutti, D. S.; Cheatham, T. E., III; Cisneros, G. A.; Cruzeiro, V. W. D.; Darden, T. A. et al. *Amber 2021*; University of California, San Francisco, 2021.
(74) Fox, T.; Kollman, P. A. Application of the RESP Methodology in the Parametrization of Organic Solvents. *J. Phys. Chem. B* **1998**, *102*, 8070−8079.
(75) Abraham, M. J.; Murtola, T.; Schulz, R.; Páll, S.; Smith, J. C.; Hess, B.; Lindahl, E. GROMACS: High performance molecular simulations through multi-level parallelism from laptops to supercomputers. *SoftwareX* **2015**, *1−2*, 19−25.
(76) Shirts, M. R.; Klein, C.; Swails, J. M.; Yin, J.; Gilson, M. K.; Mobley, D. L.; Case, D. A.; Zhong, E. D. Lessons learned from comparing molecular dynamics engines on the SAMPL5 dataset. *J. Comput.-Aided Mol. Des.* **2017**, *31*, 147−161.
(77) Swope, W. C.; Andersen, H. C.; Berens, P. H.; Wilson, K. R. A computer simulation method for the calculation of equilibrium constants for the formation of physical clusters of molecules: Application to small water clusters. *J. Chem. Phys.* **1982**, *76*, 637−649.

(78) Darden, T.; York, D.; Pedersen, L. Particle mesh Ewald: An *N* log(*N*) method for Ewald sums in large systems. *J. Chem. Phys.* **1993**, *98*, 10089−10092.
(79) Bussi, G.; Donadio, D.; Parrinello, M. Canonical sampling through velocity rescaling. *J. Chem. Phys.* **2007**, *126*, 014101.
(80) Hess, B.; Bekker, H.; Berendsen, H. J. C.; Fraaije, J. G. E. M. LINCS: A linear constraint solver for molecular simulations. *J. Comput. Chem.* **1997**, *18*, 1463−1472.
(81) Haynes, W. M. *CRC handbook of chemistry and physics*; CRC Press, 2014.
(82) Bernetti, M.; Bussi, G. Pressure control using stochastic cell rescaling. *J. Chem. Phys.* **2020**, *153*, 114107.
(83) Parrinello, M.; Rahman, A. Polymorphic transitions in single crystals: A new molecular dynamics method. *J. Appl. Phys.* **1981**, *52*, 7182−7190.
(84) Allen, M. P.; Tildesley, D. J. *Computer Simulation of Liquids*; Clarendon Press, 1989.
(85) Samulski, E. T.; Tobolsky, A. V. Some Unusual Properties of Poly-(gamma-benzyl L-glutamate) Films Cast in Strong Magnetic Fields. *Macromolecules* **1968**, *1*, 555−557.
(86) Gouilleux, B.; Moussallieh, F.; Lesot, P. Anisotropic 1H STD-NMR Spectroscopy: Exploration of Enantiomer-Polypeptide Interactions in Chiral Oriented Environments. *ChemPhysChem* **2023**, *24*, e202200508.
(87) Mölder, F.; Jablonski, K. P.; Letcher, B.; Hall, M. B.; Tomkins-Tinch, C. H.; Sochat, V.; Forster, J.; Lee, S.; Twardziok, S. O.; Kanitz, A.; et al. Sustainable data analysis with Snakemake. *F1000Research* **2021**, *10*, 33.
(88) Courtès, L.; Wurmus, R. Reproducible and User-Controlled Software Environments in HPC with Guix. *Lect. Notes Comput. Sci.* **2015**, *9523*, 579−591.
(89) Michaud-Agrawal, N.; Denning, E. J.; Woolf, T. B.; Beckstein, O. MDAnalysis: A toolkit for the analysis of molecular dynamics simulations. *J. Comput. Chem.* **2011**, *32*, 2319−2327.
(90) Gowers, R. J.; Linke, M.; Barnoud, J.; Reddy, T. J. E.; Melo, M. N.; Seyler, S. L.; Domanski, J.; Dotson, D. L.; Buchoux, S.; Kenney, I. M.; et al. MDAnalysis: A Python Package for the Rapid Analysis of Molecular Dynamics Simulations. *Proceedings of the 15th Python in Science Conference* **2016**, 98−105.
(91) Hervet, H.; Dianoux, A. J.; Lechner, R. E.; Volino, F. Neutron scattering study of methyl group rotation in solid para-azoxyanisole (PAA). *J. Phys. (Paris)* **1976**, *37*, 587−594.
(92) Dai, N.; Jones, G. Multivariate initial sequence estimators in Markov chain Monte Carlo. *Journal of Multivariate Analysis* **2017**, *159*, 184−199.
(93) Jones, G. L. On the Markov chain central limit theorem. *Probability Surveys* **2004**, *1*, 299−320.
(94) Liu, Y.; Cohen, R. D.; Martin, G. E.; Williamson, R. T. A practical strategy for the accurate measurement of residual dipolar couplings in strongly aligned small molecules. *J. Magn. Reson.* **2018**, *291*, 63−72.
(95) Goga, N.; Rzepiela, A. J.; de Vries, A. H.; Marrink, S. J.; Berendsen, H. J. C. Efficient Algorithms for Langevin and DPD Dynamics. *J. Chem. Theory Comput.* **2012**, *8*, 3637−3649.
(96) Paton, R. S.; Goodman, J. M. Hydrogen Bonding and $\pi$-Stacking: How Reliable are Force Fields? A Critical Evaluation of Force Field Descriptions of Nonbonded Interactions. *J. Chem. Inf. Model.* **2009**, *49*, 944−955.
(97) Söntjens, S. H. M.; Sijbesma, R. P.; van Genderen, M. H. P.; Meijer, E. W. Stability and Lifetime of Quadruply Hydrogen Bonded 2-Ureido-4[1H]-pyrimidinone Dimers. *J. Am. Chem. Soc.* **2000**, *122*, 7487−7493.